A short-cut-method for the quantification of crystallization kinetics - Part 2: Experimental application

Erik Temmel[1], Matthias Eicke[1], Heike Lorenz[1], Andreas Seidel-Morgenstern[1,2*]
[1]Max Planck Institute for Dynamics of Complex Technical Systems, Germany
[2] Otto von Guericke University Magdeburg, Chair of Chemical Process Engineering, Germany

Abstract

For the design of crystallization processes, the specific substances have to be characterized in terms of their thermodynamic properties but also with respect to the corresponding crystallization kinetics. In an accompanying theoretical study, a short-cut-method was suggested and demonstrated for the quantification of different kinetic mechanisms, i.e. growth, dissolution and nucleation. Here, this method will be utilized for the estimation of parameters comprised in kinetic sub-models for three different substances. The experimental procedures as well as the data analysis will be discussed and the quality of the parameter estimates will be evaluated by comparing predictions of a population balance model using the identified parameters with the results of corresponding validation experiments.

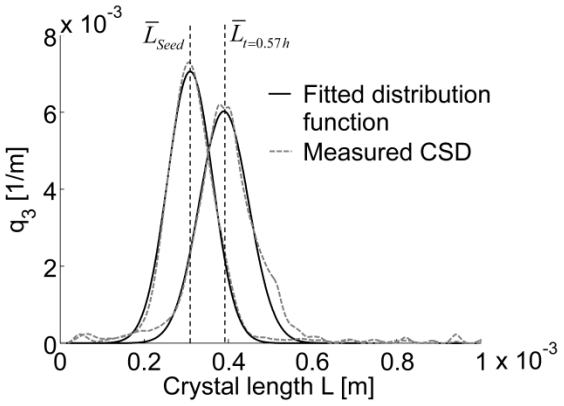

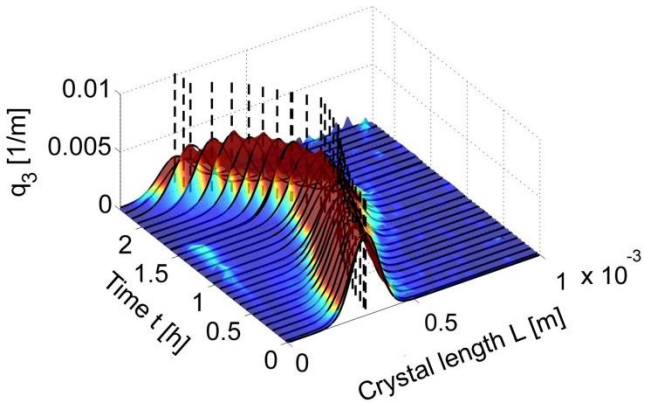

Corresponding author: Andreas Seidel-Morgenstern
Max Planck Institute for Dynamics of Complex Technical Systems; Sandtorstraße 1, 39106 Magdeburg, Germany
Tel: +49 391 6110401; Fax: +49 391 6110521
Email: seidel@mpi-magdeburg.mpg.de

A short-cut-method for the quantification of crystallization kinetics - Part 2: Experimental application

Erik Temmel[1], Matthias Eicke[1], Heike Lorenz[1], Andreas Seidel-Morgenstern[1,2*]
[1]Max Planck Institute for Dynamics of Complex Technical Systems, Sandtorstr. 1, D-39106 Magdeburg, Germany
[2]Otto von Guericke University Magdeburg, Chair of Chemical Process Engineering, Universitätsplatz 2, D-39106 Magdeburg, Germany

* Corresponding author: seidel@mpi-magdeburg.mpg.de

Abstract

For the design of crystallization processes, the specific substances have to be characterized in terms of their thermodynamic properties but also with respect to the corresponding crystallization kinetics. In an accompanying theoretical study, a short-cut-method was suggested and demonstrated for the quantification of different kinetic mechanisms, i.e. growth, dissolution and nucleation. Here, this method will be utilized for the estimation of parameters comprised in kinetic sub-models for three different substances. The experimental procedures as well as the data analysis will be discussed and the quality of the parameter estimates will be evaluated by comparing predictions of a population balance model using the identified parameters with the results of corresponding validation experiments.

Keywords: Crystallization processes, Particle size distributions, Kinetics, Nucleation, Growth, Dissolution, potassium aluminum sulfate, potassium dihydrogen phosphate, ortho aminobenzoic acid

1. Introduction

Many methods with specific assets and drawbacks are known for the quantification of kinetics [1]. Commonly desupersaturation experiments, single crystal growth cells, fluidized bed crystallizations or the MSMPR principle are applied. These methods require an extensive amount of experiments, additionally to their specific limitations [2, 3], to quantify nucleation, growth or dissolution rates for a certain range of supersaturation and temperature.
Therefore, it is convenient to measure the required information in polythermal bulk crystallizations under consideration of the liquid and solid phase evolution for practical applications [4, 5]. These experiments provide several combinations of temperature and supersaturation during one experiment and therefore an efficient investigation of the desired kinetics over the considered range of process conditions.
The first part of this study [4] demonstrated the feasibility of a simple short-cut-method exploiting *in silico* data of a few seeded batch-crystallizations. This idea will be applied in the present study to three different substance systems, namely potassium aluminum

sulphate dodecahydrate (KAL), potassium dihydrogen phosphate (KDP) and ortho aminobenzoic acid (oABA).
The first substance serves as a model component, which is well soluble and often investigated. Hence, the corresponding experiments and results are utilized to validate the data processing and the overall method.
Potassium dihydrogen phosphate is chosen since the shape of the crystals depends significantly on the applied process conditions. If only one crystal dimension (e.g. crystal length or width) is observed during the experimental investigations, a simulation utilizing the subsequently estimated parameters, describes just this dimension. Consequently, an error will occur if another dimension is predominant for certain crystallization conditions. Thus, the impact of a changing morphology on the precision of the quantified kinetic rates utilizing the short-cut-method can be investigated.
In contrary to the well soluble and well growing substances KDP and KAL, oABA represents a case close to numerous pharmaceuticals. The solubility in water is limited to 1 wt-% for the investigated temperature range. Furthermore, part of the crystal phase floats on the liquid surface during crystallization/ dissolution experiments due to the low solid density. Additionally, a lot of air bubbles were mixed into the suspension due to these floating crystals. Present crystals exhibited a strong agglomeration tendency regardless whether the process was seeded or not. Also some insoluble impurities were present in the raw material that led, together with the other facts mentioned, to a rather strong scattering of the CSD data acquired with the online microscope. Hence, this component is close to a realistic case and the specific substance properties complicate the quantification of the desired kinetics. The mentioned short-cut-method is applied to all three systems in the following. The experimental procedure with different measurement techniques, data analysis and parameter estimation as well as the validation of the quantified kinetics will be explained in detail.

2. Short-cut-method

The idea, which will be discussed in this contribution, is to use easily available experimental information about crystallization processes that can be acquired performing a few well planned cooling batch-experiments to quantify 1-dimensional crystallization kinetics [4]. The main task is therefore not to elucidate the underlying mechanism in detail but to provide sufficient information for a process design.

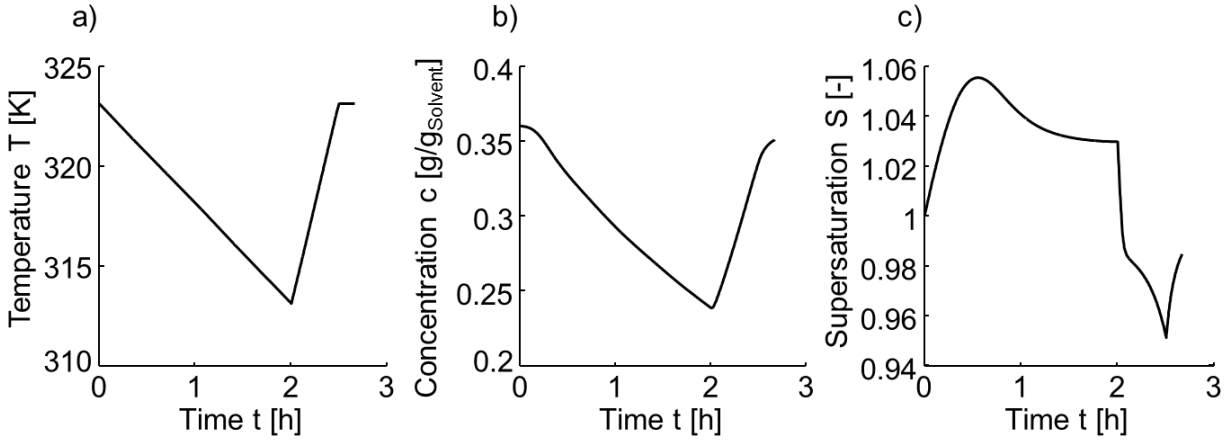

Fig. 1: Ideal hypothetical measurements of temperature, solute concentration as well as the resulting supersaturation [4].

The procedure is based on seeded cooling batch-crystallizations that are analyzed with respect to the liquid and solid phase evolutions (ideal *in silico* profiles are shown in Fig. 1). A similar approach can be utilized to estimate 3-dimenstional growth and dissolution kinetics as well [5, 6] but with larger numerical effort due to a shape estimation procedure. Furthermore, different sets of experiments with defined constant conditions were utilized e.g. in [6]. Hence, the presented short-cut-method is intended to reduce the experimental and numerical effort, the complexity of the data evaluation and the measurement technique requirements to quantify the nucleation, growth and dissolution kinetics.

.

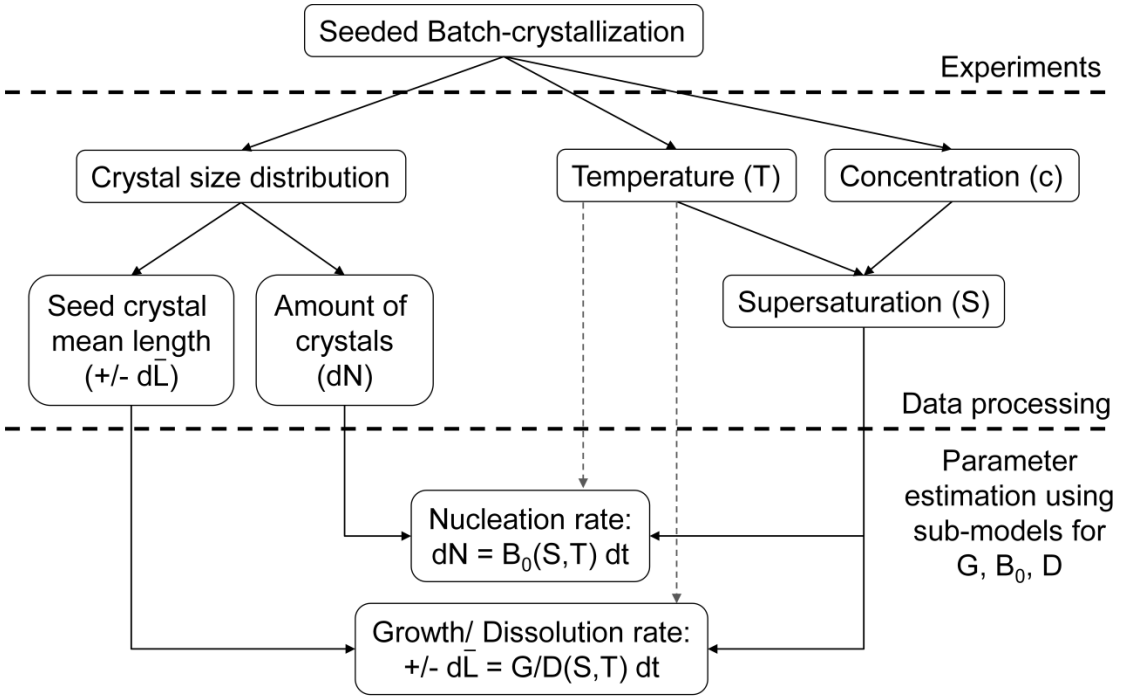

Fig. 2: Principle of the proposed short-cut method [4].

The experiments are assumed to start from a slightly supersaturated solution that is cooled further after the seeds are added. Samples are taken during the experiment to analyze the CSD with an appropriate measurement technique (e.g. sieve analysis, online microscopy). Nucleation will take place and the initial crystals will grow as long as supersaturation is present. Subsequently, the mean length ($\bar{L}$) of the growing seed fraction is extracted from the CSDs as input information for the parameter estimation of the growth kinetics (Fig. 2, *G*). The relative supersaturation (*S*, Fig. 1 c) during the crystallization process is calculated [4] based on the temperature (*T*, Fig. 1 a) and the measured concentration (*c*, Fig. 1 b), together with a preliminarily determined solubility curve. Subsequently, the parameters of a specific kinetic sub-model are varied under consideration of supersaturation and temperature to match the observed mean length changes.

Additionally, all present crystals in the CSD samples are counted to observe the change of the total amount of particles (Fig. 2, *N*) during the crystallization. Afterwards, the parameters of a nucleation (Fig. 2, B_0) sub-model are fitted to this data.
The same procedure described for the growth kinetics can be applied to quantify the dissolution rate (Fig. 2, *D*) as well, while undersaturation is present (e.g. due to heating).

3. Experiments

The short-cut-method is applied to the three binary substance systems, potassium alum, potassium dihydrogen phosphate and ortho aminobenzoic acid dissolved in water. The set-up, which is used for the cooling crystallizations, the specifications of the utilized measurement techniques and the purchased material, are described in the following.

3.1. Set-up

The reactor utilized for the experimental investigations is a double jacket draft tube baffle crystallizer with an inner volume of 25 L (Fig. 3). It is equipped with a refractive index probe (Fig. 3, RI, PR-23, K-Patents) and a Pt100 (Fig. 3, T) for the inline concentration and temperature analysis of the liquid phase. Additionally, the liquid concentration is determined offline after periodic sampling with a gravimetric or HPLC analysis (HP 1200, Dionex) to verify the inline measurement. Appropriate mixing of the solid and liquid phase is ensured by a propeller stirrer.
Two different options for the analysis of the CSD are present at the utilized set-up. One is an online microscope (QicPic, Sympatec) connected to the crystallizer via thermostated tubes and a peristaltic pump (IP 65, Ismatec). The unclassified suspension is withdrawn from the crystallizer and introduced into a flow-through-cell of 2 mm width. The microscope records 25 images per second of the suspension in a field of view of 5-by-5 mm. All images are evaluated automatically with the image processing toolbox pre-programmed in Matlab (Mathworks) and a modified algorithm described in [7] with respect to the observed single crystals. Thus, the CSD is measured without any further treatment of the suspension.
Even though, this technique is precise and reliable, crystals which are bigger than 1.0 - 1.5 mm cannot be investigated due to sedimentation inside the flow-through-cell. Furthermore, the saturation temperature limit for the device is 35°C - 40°C since the cell cannot be tempered and blockage of the suspension flow can occur.
Thus for the second option, the bottom outlet is utilized to investigate the solid phase if higher concentrated solutions are present or bigger crystals have to be investigated. The suspension is withdrawn unclassified from the crystallizer via the pneumatic valve and subsequently washed, filtered and dried appropriately. A sieve analysis is utilized afterwards to determine the CSD of the sample.

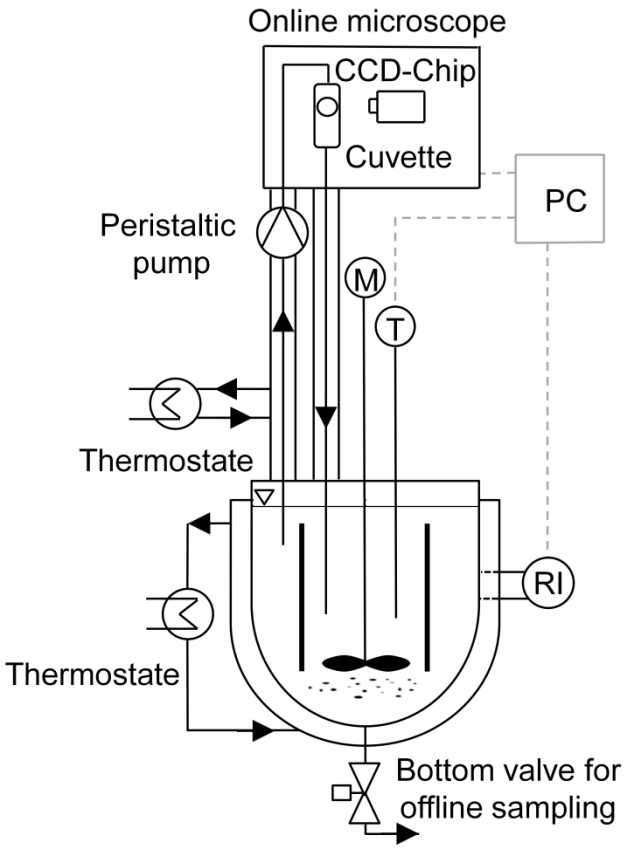

Fig. 3: Scheme of the utilized experimental set-up. The 25 L crystallizer is equipped with temperature (T) and concentration (refractive index probe, RI) measurement devices for the liquid phase analysis. An online microscope and a non-classifying bottom outlet can be used for the investigation of the solid phase.

3.2. Analyses

The refractive index (RI) probe was used to investigate the solution concentration of both salt systems during the experiments. Since the refractive index depends on temperature as well, a 2-dimensional calibration was performed over a temperature range of θ = 20°C…60°C and a concentration range of c = 0…c*(60°C). A polynomial function (c = f(RI, θ)) was fitted to the corresponding data and subsequently applied to reconstruct the solution concentration from the continuous measurement signal.

The ortho aminobenzoic acid concentration could not be measured precisely with the refractive index probe. Thus, an offline HPLC (Dionex HP 1200, Thermo Scientific) method was utilized for determination of the liquid phase concentration. The system was equipped with a Kinetex C18 column (Phenomenex, length 250 mm, diameter 4.6 mm, particle diameter 5 µm). Acetonitrile/ water (80/ 20) served as the eluent. Samples were injected at a flow rate of 0.5 ml/min and a temperature of 25 °C with an injection volume of 1 µl. The average observed retention time of oABA was 5.77 min.

Necessary CSD information were extracted from recorded images of the online microscope and from the sieve analysis. The latter one is a rather old and well known

technique often used for particle analysis. It is assumed, that the second largest dimension of the crystals defines the sieve mesh size that it can pass. Thus, this dimension is the basis for the measured CSD.
Suspension samples taken during the process were filtered, washed and dried appropriately. The solid phases were subsequently sieved using 23 sieves (Analytical sieves, Retsch) with mesh sizes from 63 µm to 2000 µm placed on a mechanical shaker (AS200 digit, Retsch), which was run for 15 min at a frequency of 60 Hz. The sieve fractions were weighed afterwards yielding the corresponding mass distribution.
Microscopic investigations are more complex with respect to the CSD analysis. The evaluation of images recorded by the online device (Fig. 4, *left*) is roughly divided into 3 steps: image enhancement (Fig. 4, *middle*), thresholding and region filling as well as particle identification and measurement [5] (Fig. 4, *right*).

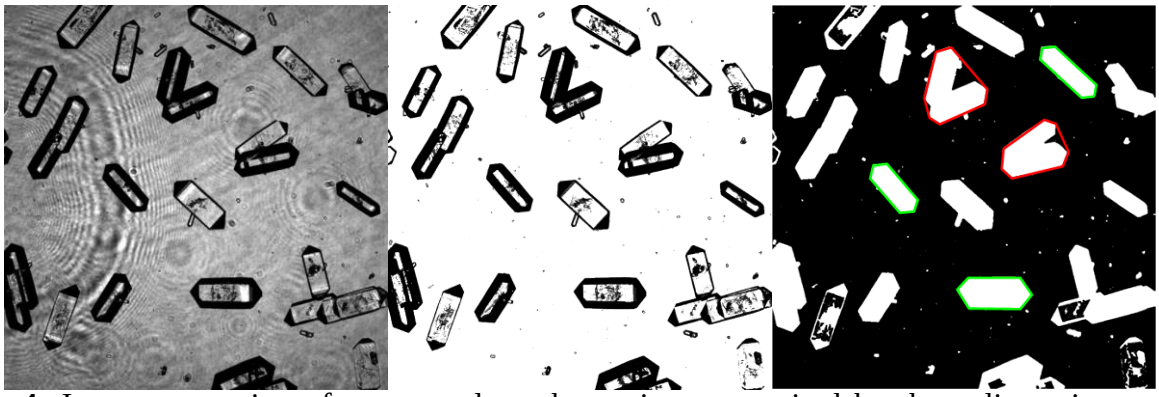

Fig. 4: Image processing of an exemplary chosen image acquired by the online microscopy. From left to right: Original image, background removal, binarization and single crystal identification.

At first, the grey background is removed from the original image to enhance the visibility of the particles (Fig. 4, *middle*). Afterwards, the image is binarized by a global grey-scale threshold yielding a black background and well distinguishable white particles (Fig. 4, *right*). Small gaps and holes can appear in the black and white image at the inside or at the boarder of the particle shadows due to transparency of the original crystals. These regions are subsequently filled by appropriate morphological closing operators pre-programmed in the image processing toolbox that is implemented in MatLab (Mathworks). Finally, the boundary curve of all visible particles can be extracted (Exemplarily shown for a few particles as *red and green lines* in Fig. 4 *right*). Only the single crystals are evaluated for the CSD (*green lines* in Fig. 4 *right*) and agglomerates (*red lines* in Fig. 4 *right*) and air bubbles are excluded automatically to a certain extent by utilization of characteristic morphological factors, e.g. sphericity and convexity. Particles touching the boarder of the image are ignored for the evaluation. Additional details about the algorithm can be found elsewhere [7].
For comparison with the sieve analysis, the minimal Ferret-diameter of the extracted boundary curve was utilized for the size evaluation of the observed particles that yields the number density distribution, *f(L)*.
The solid phases were additionally analyzed with respect to the occurring phases by X-Ray Powder Diffraction applying an X'Pert Pro Diffractometer (PANalytical GmbH,

Germany) in a 2-Theta range between 20 and 80°, with a step size of 0.008° and a step time of 120s.

3.3. Materials

Potassium alum (KAL) was purchased from Applichem and potassium dyhidrogen phosphate (KDP) from Carl Roth, both with a purity of >98%. Ortho aminobenzoic acid (oABA) was bought from VWR with a purity of >99%. The solvent for all three solutes was deionized water.
The solid densities and the later applied volumetric shape factors, k_V (see Appendix for calculations), of these substances crystallized from water (Fig. 5) are listed in table 1.

Table 1: Substance characteristics of the investigated binary systems.

	Symbol	KAL (hydr.)	KDP	oABA	Unit
Solid density	ρ_{solid}	1750	2340	1380	[kg/m^3]
Volumetric shape factor (see Appendix)	k_V	√2/3	0.75 (avg.)	0.32(±0.06)	[-]
Molar mass	$\tilde{M}$	474.39	136.09	137.14	[g/mol]
Purity	Pr	≥99.5%	≥98%	≥99	[%]
Distributor		Applichem	Carl Roth	VWR	

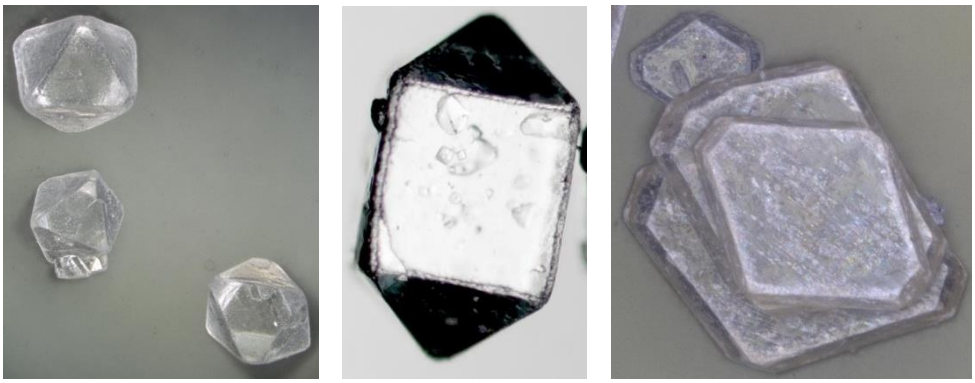

Fig. 5: Typical crystal shapes of potassium alum sulphate, potassium dihydrogen phosphate and ortho aminobenzoic acid crystallized from water (from left to right).

4. Procedures

The basis for all crystallization processes is the solid-liquid-equilibrium. It was measured for all three substances and will be given in the following. Furthermore, the experimental procedure will be explained.

4.1. SLE-measurements

The saturation curves of potassium dihydrogen phosphate and potassium alum in water were measured applying an isothermal technique. Samples were taken from equilibrated suspensions in a temperature range of 10°C - 70°C and analyzed gravimetrically. The solubility of ortho aminobenzoic acid was determined in [8] applying the same method as for the salt systems in a range of 20°C - 60°C. The samples were analyzed with respect to the saturation concentration utilizing the HPLC method described in section 3.2. for this substance. Subsequently, polynomial expressions (eq. 1) were fitted to the solubility data of the three substance systems. The determined saturation curves are depicted in figure 6 together with data from literature [9]. The corresponding parameters are listed in table 2. With these information, the crystallization experiments were planned and carried out.

$$c^* = p_{S,1} + p_{S,2}\theta + p_{S,3}\theta^2 + p_{S,4}\theta^3 + p_{S,5}\theta^4 \qquad \text{(eq. 1)}$$

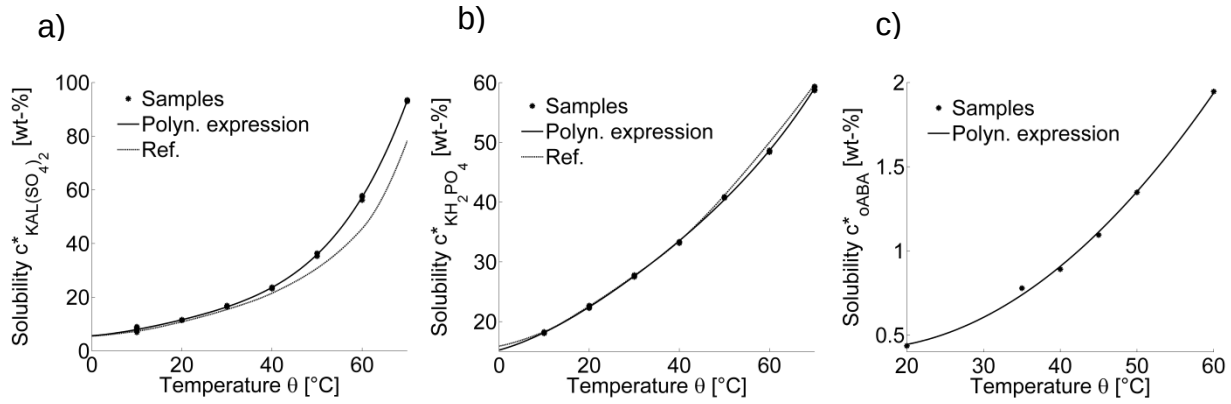

Fig 6: Measured solubilities in comparison with literature data [9] of potassium aluminum sulfate dodecahydrate (a) and potassium dihydrogen phosphate (b) together with the corresponding polynomial expression (eq. 1). Solubilty of ortho aminobenzoic acid (c) taken from [8] together with the corresponding polynomial expression (eq. 1).

Table 2: Solubility parameters of potassium alum, potassium dihydrogen phosphate and ortho aminobenzoic acid corresponding to eq. 1.

Parameter	$KAL(SO_4)_2$	KH_2PO_4	oABA [5]	Unit
$p_{S,1}$	5.06	15.24	5.48×10^{-1}	[wt-%]
$p_{S,2}$	0.23	2.06×10^{-1}	-1.93×10^{-2}	[wt-%/°C]
$p_{S,3}$	7.76×10^{-3}	1.01×10^{-2}	7.09×10^{-4}	[wt-%/°C^2]
$p_{S,4}$	-2.43×10^{-4}	-1.45×10^{-4}	0	[wt-%/°C^3]
$p_{S,5}$	4.86×10^{-6}	1.23×10^{-6}	0	[wt-%/°C^4]

4.2. Experimental procedure

The seeded batch-crystallizations were carried out with the set-up described in section 3.1. At first, solutions of the corresponding substances, saturated at the indicated temperatures, T_{Sat}, were created (see Table 3 and Fig. 7). The mass of initial material, m_{Solute}, was mixed for 30 min with the corresponding mass of solvent, m_{H2O}, at 10 K above saturation temperature to ensure complete dissolution. Before seeds were added (t_0 in Fig. 7), all solutions were subcooled by 1 K (T_0 in Fig. 7).

Subsequently, different linear cooling and heating ramps (ΔT/ Δt in Table 3) were applied to generate the corresponding driving force for crystallization. As expected the real temperature profiles exhibit a certain delay behavior contrary to *in silico* data (compare Fig. 7 a) and Fig. 1 a). The stirring rate was set to 300 rpm in all cases.

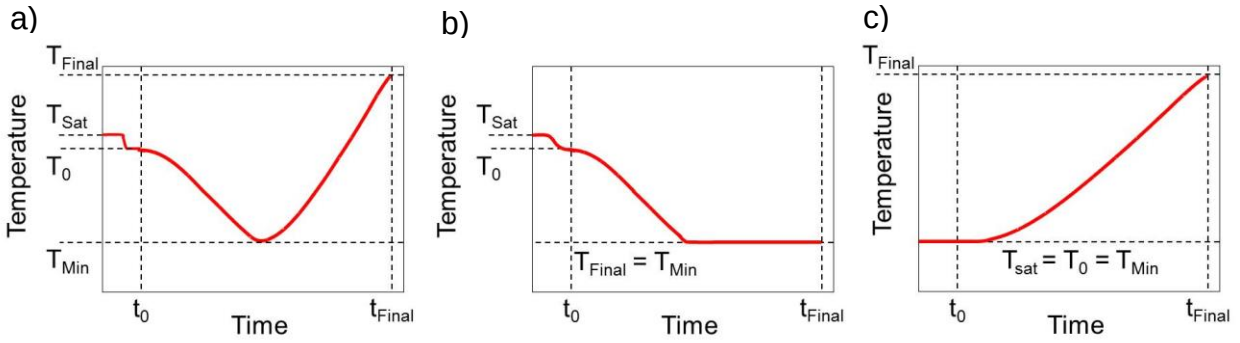

Fig 7: Illustrations of the different temperature scenarios that were applied for the investigations of the three substance systems; a) Linear cooling with subsequent linear heating to investigate growth and dissolution of the seed fraction (G/ D in Table 3); b) Simple linear cooling to investigate only growth of the seed fraction (G in Table 3) or primary nucleation (Pri. nuc. in Table 3); c) Simple linear heating to investigate dissolution of the seed fraction (D in Table 3).

It is essential for the short-cut-method to generate sufficient supersaturation during the experiments to be able to observe an appropriate growth of the seed crystals (for the dissolution kinetics *vice versa*). Nevertheless, extremely high levels of supersaturation should be avoided as well, since strong nucleation complicates the evaluation of the growing seed fraction. Thus, the cooling rates were chosen accordingly for every substance. Furthermore, for the three substance systems, slightly different experimental procedures were applied, which are detailed in the following.

Potassium alum was investigated with the online microscope (exp. KAL_1- KAL_4) and offline, using sieve analysis (exp. KAL_5- KAL_{11}). For the online analysis (exp. KAL_1- KAL_4), cooling rates of -5 and -10 K/h as well as 100 g of seed crystals with a mean size of 250 µm were chosen. This procedure provided a good tracking of the seed fraction and enough supersaturation to investigate growth together with secondary nucleation behavior. A subsequent heating ramp of 15 K/h was applied to additionally investigate dissolution within the same experiment (Fig. 7 a) and G/ D in Table 3). The cooling ramp was stopped at T_{Min} (see Table 3 and Fig. 7) when either the seed crystals grew too large and thus, started to settle inside the flow-through cell, or crystallization inside the cell blocked suspension flow. The final temperature of the experiments (T_{Final} in Table 3 and Fig. 7) was chosen to ensure a complete dissolution of the seed crystals.

For the offline investigation of the CSD evolution (exp. KAL_5- KAL_{11}), sufficient solid material had to be provided for a precise sieve analysis. Thus, an average suspension volume of 300 ml was withdrawn via the bottom valve and processed as described in section 3.2. The volume reduction due to sampling must not change the fluid dynamics inside the draft tube crystallizer significantly. Thus, only a limited amount of samples was taken during one experiment. Therefore, growth and secondary nucleation kinetics had to be investigated separately from the dissolution kinetics during a different set of experiments (Fig. 7 b) and c) whenever sieve analysis was applied.
Additionally, the seeding strategy had to be adjusted to the resolution of the sieve analysis. For the growth experiments, 400 g of crystals with a mean length of 550 µm were used. Due to the initially higher crystal surface, the cooling rate was increased to -15 K/h to generate enough supersaturation. For the dissolution experiments, seed crystals with a mean length of 1 mm were used. The initial mass was calculated to create a saturated solution after the final temperature (T_{Final}). Even though, the experimental effort for the sieve analyses was higher than for the online microscopy, higher temperatures as well as larger crystals could be investigated.
The procedure for the investigation of potassium dihydrogen phosphate (KDP_1- KDP_4) was similar to the experiments with KAL where the online microscope was used. It is known, that the shape of KDP crystals strongly depends on supersaturation during crystallization [5, 6]. Thus, the cooling and heating rates were increased for the KDP experiments to additionally investigate the impact of the shape change on the results of the short-cut method. Similar to the (KAL_1- KAL_4) experiments, 100 g of seed crystals with a mean length of 250 µm were used.
The general investigation of ortho aminobenzoic acid ($oABA_1$-$oABA_5$) was carried out in a similar way as the KDP experiments with a seeding strategy adapted to the low solubility of the substance (Fig. 7 c). Only 1.6 g to 16 g of seed crystals with a mean length of 77 µm were provided to ensure good visibility of the growth of these crystals. Furthermore, experiments from clear solutions were carried out (temperature profile Fig. 7 c) for this substance to investigate the primary nucleation behavior (Pri. nuc. in Table 3).
For every substance system, a validation experiment (KAL_{Valid}, KDP_{Valid}, $oABA_{Valid}$ in Table 3) was performed that was not utilized during parameter estimation. The comparison between the measured quantities of these experiments and a model prediction using the quantified kinetic rates will serve as an evaluation of the short-cut-method and the estimates.
The observations of selected experiments from table 3 as well as the results of the parameter estimations will be discussed in the following.

Table 3: Experimental procedures for the substances potassium alum (KAL), potassium dihydrogen phosphate (KDP) and ortho aminobenzoic acid (oABA). The investigated kinetics (primary nucleation (*Pri. nuc.*), growth (*G*), and dissolution (*D*)) are listed together with the cooling and heating ramps, initial saturation temperature and corresponding substance masses. Highlighted experiments are presented and intensively discussed in the following.

Sampling method	Exp.	Investigated kinetics	ΔT/ Δt [K/h]	T_{Sat} [K]	T_{Min} [K]	T_{Final} [K]	m_{H2O} [kg]	m_{Solute} [kg]	m_{Seeds} [kg]
Online microscopy	KAL_1	G/ D	-5/ +15	303	296	306	21	3.5	0.1
	KAL_2	G/ D	-10/ +15	303	296	306	21	3.5	0.1
	KAL_3	G/ D	-5/ +15	308	299	314	20	4	0.1
	KAL_4	G/ D	-10/ +15	308	295	314	20	4	0.1
	$KAL_{Valid.}$	G/ D/ G	-10/ +15/ -5	308	299	299	20	4	0.1
Sieve analysis	KAL_5	G	-15	335	292.5	292.5	17.5	10.5	0.4
	KAL_6	G	-15	325	292.3	292.3	19	7.5	0.4
	KAL_7	G	-15	315	293	293	21	5.6	0.4
	KAL_8	G	-15	305	293	293	22.5	4	0.4
	KAL_9	D	+15	313	313	333	16	3.9	5.2
	KAL_{10}	D	+15	293	293	333	18	2	8.3
	KAL_{11}	D	+15	293	293	315	20	2.2	3
Online microscopy	KDP_1	G/ D	-10/ +20	303	296	309	21	5.9	0.1
	KDP_2	G/ D	-16/ +20	303	295	310	21	5.9	0.1
	KDP_3	G/ D	-5/ +20	303	297	310	21	5.9	0.1
	KDP_4	G/ D	-16/ +20	308	300	314	21	6.5	0.1
	$KDP_{Valid.}$	G/ D/ G/ D	-10/ +20/ -5/ +20	308	300	314	21	6.5	0.1
Online microscopy	$oABA_1$	Pri. nuc.	-10	308	292.5	292.5	23	0.17	0
	$oABA_2$	G/ D	-10/ +11	308	292.6	312	23	0.17	$16X10^{-3}$
	$oABA_3$	Pri. nuc.	-11	308	292.6	292.6	23	0.17	0
	$oABA_4$	G	-5	312	292.6	292.6	23	0.2	$16X10^{-4}$
	$oABA_5$	G/ D	-7.5/ +11	312	292	314	23	0.2	$16X10^{-4}$
	$oABA_{Valid.}$	Pri. nuc.	alternating	313	293	293	23	0.21	0

5. Results and discussions

In the following the data analysis, parameter estimation as well as the model validation will be discussed in detail for potassium alum. For the other substances only the parameter estimates and the model prediction in comparison with the measurements of the validation experiments are given to avoid unnecessary repetitions.

5.1. Data analysis

Figure 8 shows, as an example, the measurements of experiment KAL_1 where a linear cooling ramp of -5 K/h and a linear heating ramp of 15 K/h was used (see Table 3).

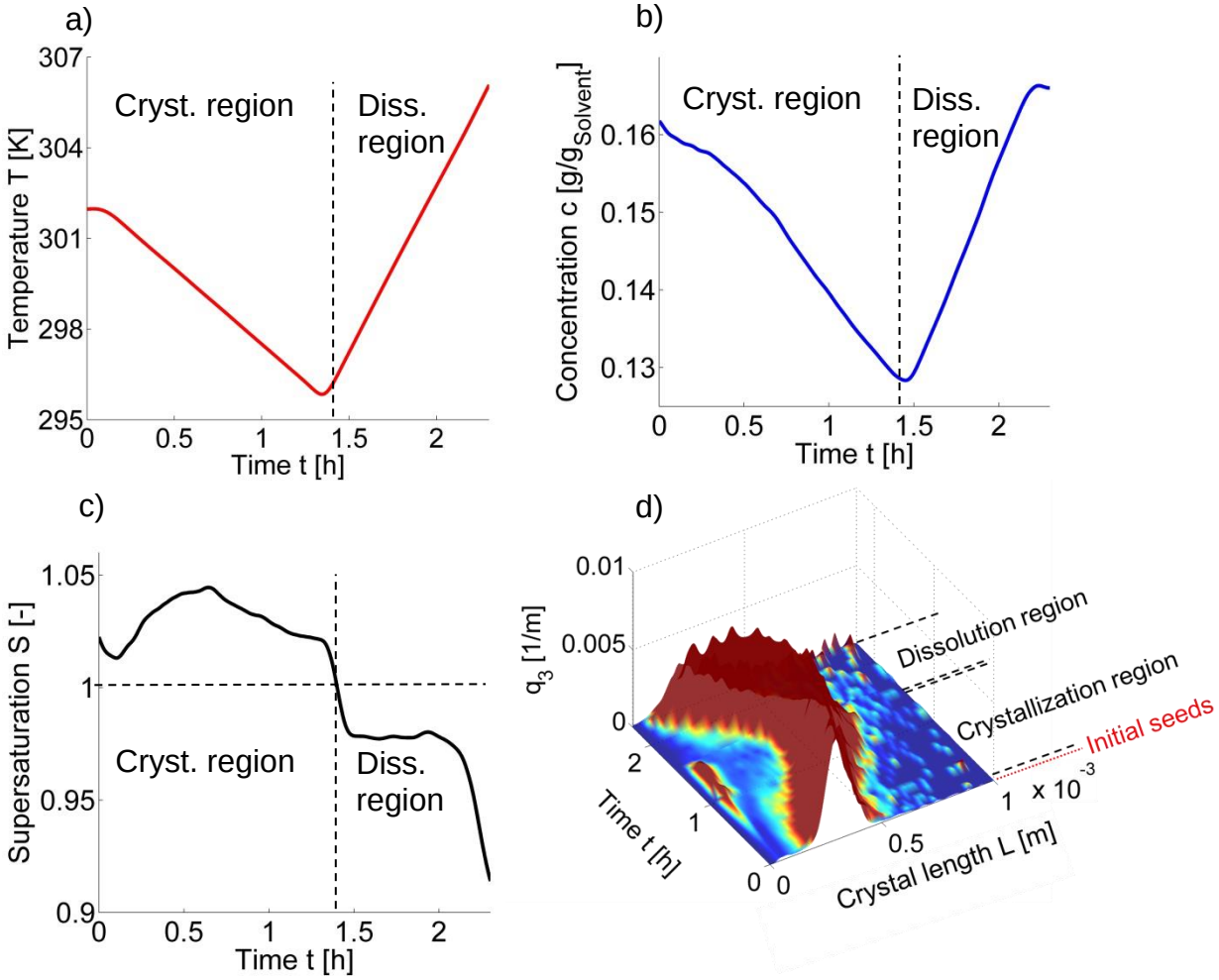

Fig 8: Measured data of experiment KAL_1; a) Temperature (scenario Fig. 7 a); b) Concentration trajectory determined from the refractive index probe; c) Calculated transient supersaturation; d) Observed CSD evolution depicted as a mass density distribution, q_3 (eq. 3).

After seeding at t = 0, the concentration starts to decrease as expected (Fig. 8 b). The decrease of the liquid phase concentration accelerates once cooling is initiated.
The transient supersaturation depicted in figure 8 c) was calculated using the temperature profile (Fig. 8 a), the concentration and the corresponding solubility curve

(Fig. 6 a). It can be seen that due to cooling, a maximum of 5 % supersaturation in the crystallization region and as a result of the subsequent heating a minimum of 2 % undersaturation in the dissolution region is reached.
The measured CSD evolution from the recorded images of the online microscopy is shown in figure 8 d) as a mass density distribution, q_3 (eq. 2).

$$q_3(L) = \frac{L^3 f(L)}{\int_0^\infty L^3 f(L) dL} \qquad \text{(eq. 2)}$$

During cooling, the seed crystals grow to a final size of around 550 µm until undersaturation is present (t = 1.4 h). Subsequently, the crystals dissolve and the average crystal length decreases.
Additionally, secondary nucleation occurs in the crystallization region at L < 100 µm (Fig. 8 d)). Apparently, most of these new crystals exhibit a much lower growth rate than the initial seeds. This behavior is commonly known as growth rate dispersion (GRD). It can be caused by e.g. tensions inside the crystal lattice resulting from the collision of the mother crystals with the stirrer or other objects inside the reactor during the secondary nucleation process, a phenomenon described for example in [10].
The seed crystal fraction broadens due to GRD during the course of the process, which leads to change of the standard deviation of seed distribution. Nevertheless, this does not influence the presented method since only the crystal mean length is utilized as the input information to estimate the growth parameters [4].
Furthermore, outliers are visible (small peaks at L>500 µm) that are most likely caused by agglomerates or air bubbles which passed the image processing routine.
Especially secondary nucleation, breakage, agglomeration and outliers are challenging for the quantification of the growth rate since the short-cut-method requires an accurate calculation of the mean size of the seed fraction. Therefore, a distribution function, which initially describes the seeds best, is chosen and then fitted to a part of the observed CSD that most likely contains the growing seed fraction. Hence, an objective mean length of the growing seed fraction can be calculated (eq. 3) that is not influenced by other effects.
This procedure is explained using two observed CSDs as an example (Fig. 9 a). The left distribution depicts the initial seeds (grey dashed line), which can be described best with a Gaussian distribution (black solid line). It can be seen from the CSD on the right that agglomerates (small shoulder at L = 500 µm in Fig. 9 a), secondary nuclei and outlier can be isolated from the seed fraction when the distribution function is fitted appropriately. In contrary to ideal data [4], extremum and inflection points cannot be exploited to identify the grown seed fraction automatically. Hence, the seed peak had to be identified empirically for the fitting procedure. All observed CSDs are processed as described yielding the evolution of the mean length (black dashed lines in Fig. 9 b) of the seed fraction.

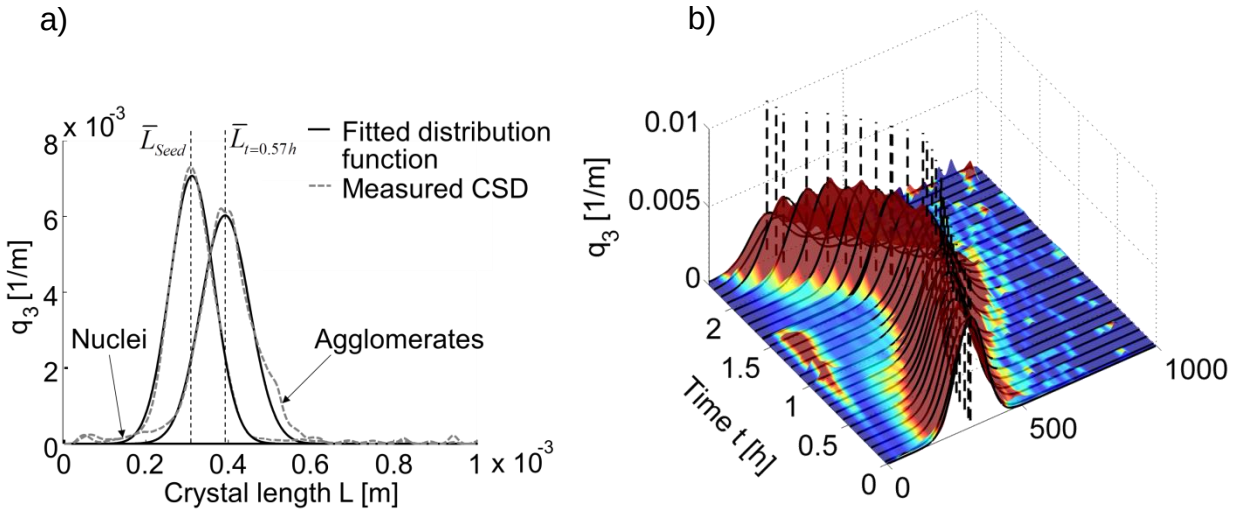

Fig 9: Measured CSD of experiment KAL_1 from the online microscopy; a) Initial CSD and CSD at t = 0.57 h (grey dashed lines) with two fitted Gaussian distribution functions (black solid lines); b) Overall CSD evolution and calculated mean values (eq. 3) of the seed fraction (black dashed lines).

$$\bar{L} = \frac{\int_0^\infty L f(L) dL}{\int_0^\infty f(L) dL} \qquad \text{(eq. 3)}$$

The calculated evolution of the trend of the mean length, $\bar{L}$,of the seed fraction for experiment KAL_1 is depicted in figure 10 a). Additionally, all measured crystals are counted, which yields the total particle number evolution (Fig. 10 b). These transient solid phase quantities are the basis for the subsequent parameter estimation, which will be explained in the next section.

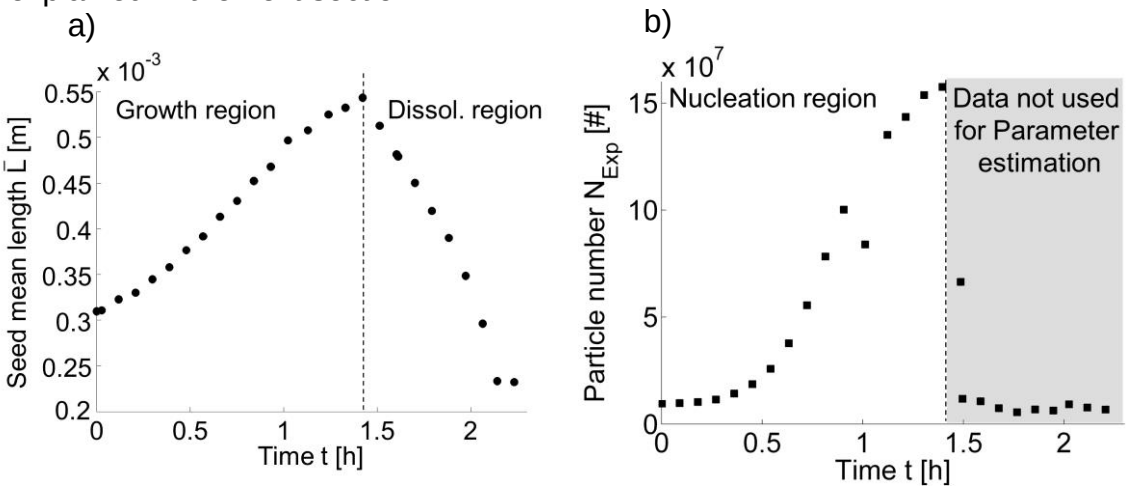

Fig 10: Evolution of the seed mean length, $\bar{L}$, and the total particle number of experiment KAL_1 after processing the observed CSDs.

Similar data can be extracted from sieve analysis as well (Fig. 11). Even though this technique is limited in precision, the movement of the seed fraction is clearly visible for the crystallization case (Fig. 11 a) and for the dissolution case (Fig. 11 b). Thus, the procedure explained for the online microscopy is applied for the sieve analysis as well, which yields the evolution of the mean length of the seed fraction. Nevertheless, it was not possible to precisely determine the overall particle amount from the sieve fraction weights. Thus, no nucleation rate can be estimated from this data.

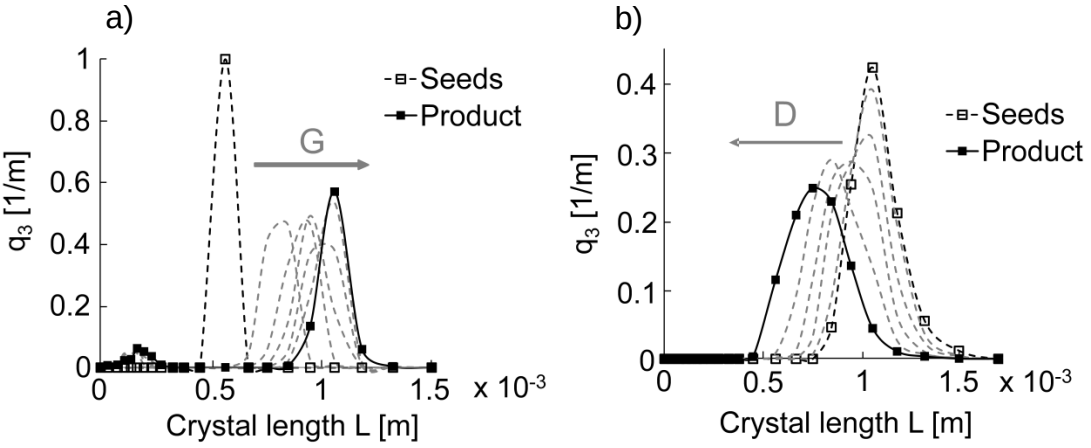

Fig 11: Sieve analysis of all samples taken during experiments KAL_7 (left) and KAL_9 (right) with indicated directions of growth and dissolution.

5.2. Parameter estimation

As shown in figure 2, the recorded data from the seeded batch crystallizations, with exception of the validation experiments, was processed and then used for parameter estimation. The driving force (e.g. super- or undersaturation) and the temperature signal are applied together with appropriate sub-models to yield the model predictions for the different kinetics ($\bar{L}_{sim}$ and N_{sim}). The parameters comprised in the sub-models are then varied to match the transient seed fraction mean length and particle number evolution ($\bar{L}_{exp}$ and N_{exp}). It is important to note that no full population balance model was applied for the parameter estimation and all kinetic sub-models were fitted separately to their corresponding data set. Additionally, no mass balance was involved in the fitting procedure as well.

Only main equations are given here. For more detailed information about the objective functions and the calculation of the theoretical values ($\bar{L}_{sim}$ and N_{sim}) for the parameter estimation see [4]. A temperature dependent power-law was chosen to describe the kinetics of growth and nucleation (eq. 4). Additionally, a sub-model that depends on the solid content, *M*, in the crystallizer (eq. 5), was applied as well since it accounts for secondary nucleation. For the validation experiments the sub-model was chosen that gave the best fitting result with respect to the objective function during parameter estimation. Also the amount of parameters was reduced in all kinetic approaches, whenever simplification lead to a similar or even better quality.

$$K = p_1 \exp(\frac{-p_2}{RT})(S-1)^{p_3} \quad \text{for K = G, D, } B_0 \quad \text{(eq. 4)}$$

$$B_0 = p_1 (S-1)^{p_2} M^{p_3} \quad \text{for secondary nucleation} \quad \text{(eq. 5)}$$

with

$$M = \frac{(c^*(T_{Sat} - 273.15K) - c) \cdot m_{H2O} + m_{Seeds}}{V_{Reactor}} \quad \text{(eq. 6)}$$

With these sub-models, the values of $\bar{L}_{sim}$ and N_{sim} in the objectives can be calculated. The best fitting result (parameters in table 4) achieved for potassium aluminum sulfate is shown exemplarily for experiment KAL_1 in figure 12.

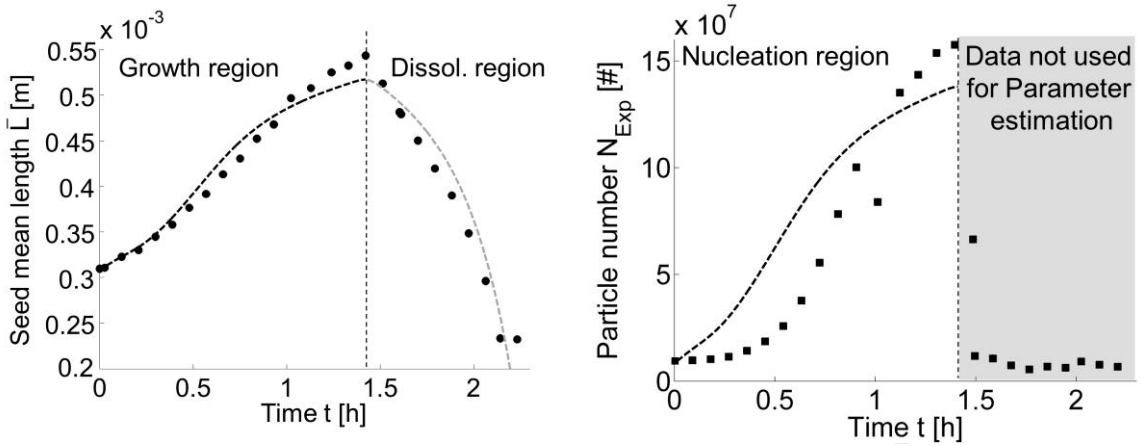

Fig. 12: Fitting results for the evolution of the seed mean length, $\bar{L}$, and the total particle number shown for experiment KAL_1; *Dots and squares:* experimental observations; *Dashed lines:* predictions of the temperature dependent sub-models (eq. 4) for the different kinetics.

A power- law with three parameters (p_1, p_2 and p_3 in eq. 4) was frequently found to best describe nucleation and growth whereas a linear, temperature independent approach is sufficient for dissolution kinetics [2]. Nevertheless, it can be seen from the estimated parameter values in table 4 that the temperature dependence of nucleation and growth is almost negligible.

Table 4: Kinetic parameter values of the power-law sub-model (eq. 4) estimated for potassium aluminum sulphate (numerical optimization method: Nelder-Mead simplex algorithm, for the complete optimization procedure see [4]) applying the CSD results from online microscopy and the sieve analysis.

Sampling method	Exp. (Table 3)	Kinetic	p_1 [m/s; 1/s]	p_2 [kJ/mol]	p_3 [-]
Online microscopy	KAL_1-KAL_4	**Growth G**	1.7×10^{-6}	5.7×10^{-9}	1.04
		Nucleation B_0	12.3×10^{5}	5.2×10^{-11}	1.1
		Dissolution D	4.3×10^{-6}	0	1
Sieve analysis	KAL_5-KAL_{11}	**Growth G**	6×10^{-6}	4.5×10^{-7}	1.4
		Dissolution D	4.5×10^{-6}	0	1

5.3. Model validation for Potassium aluminum sulphate

For evaluation of the quantified kinetics, a validation experiment, KAL_{Valid} (Table 3), was carried out that did not serve as additional input information during the parameter estimation procedure. It consisted of several cycles of crystallization and dissolution to have a qualitative difference to the experiments, which were utilized for the quantification of the kinetics. Additionally, a model prediction of the validation experiment was carried out using the estimated kinetic parameters and a full 1-dimensional population balance model [4]. The measured temperature profile, the initial concentration and the seed distribution served as the input for the simulation.
The measurements from the validation experiment with potassium alum - temperature, concentration and the CSD - are given in figure 13 along with the corresponding model predictions, which are based on the estimated parameters given in table 4.

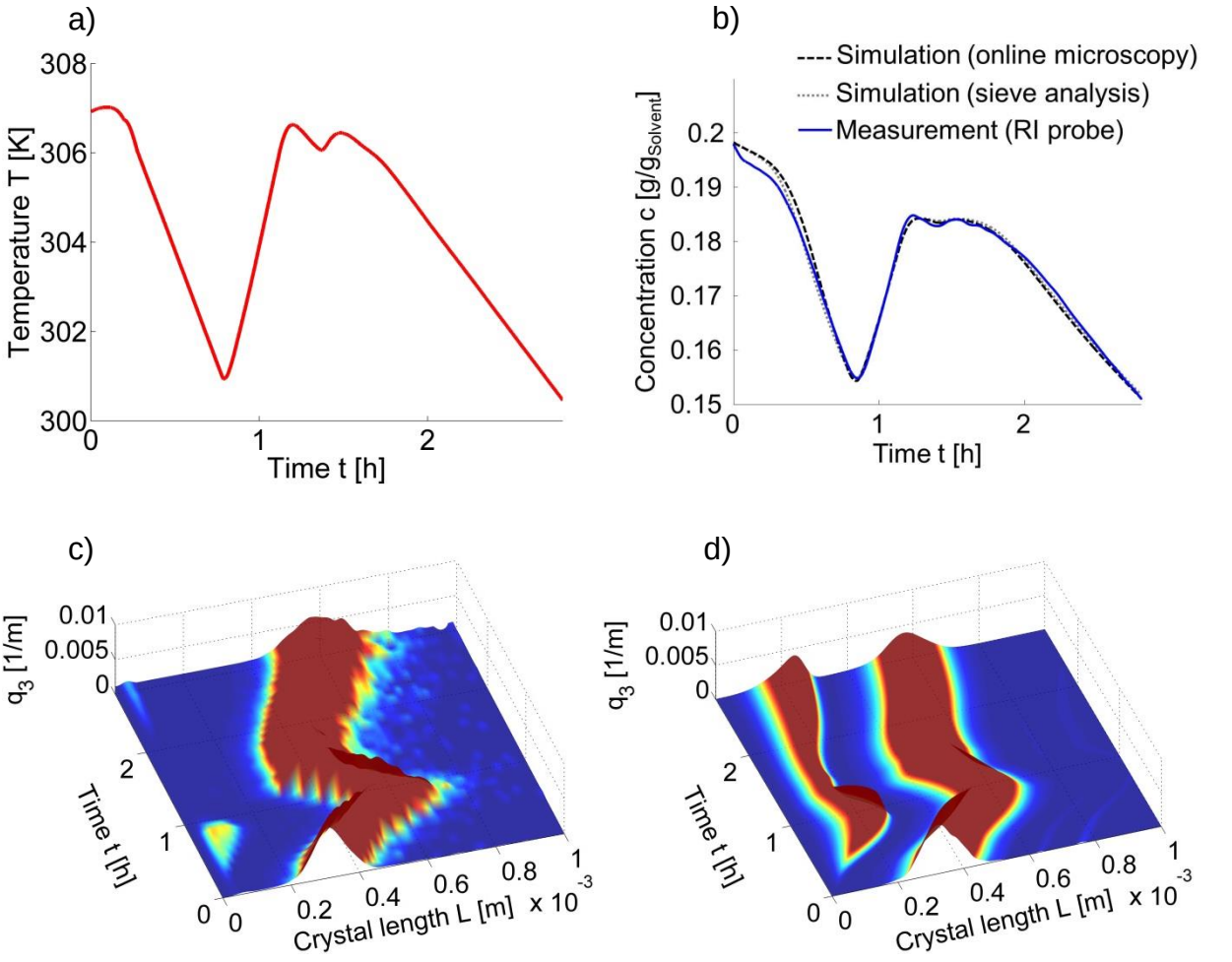

Fig. 13: Measured quantities of the validation experiment KAL_{Valid} in comparison to the model equipped with the estimated parameters from table 4; a) Temperature; b) Measured and simulated concentration profile; c) Observed CSD (online microscopy); d) Predicted solid phase evolution.

Two different kinetic parameter sets were utilized for the simulations. The first set for growth, nucleation and dissolution, results from the online microscopy measurements (Fig. 13 b), Simulation (online microscopy)). In case of the sieve analysis a complete model parameterization is not possible since nucleation cannot be determined to a suitable degree of accuracy with this method. Instead, the quantified nucleation rate obtained from the online microscopy is applied to validate the estimated growth and dissolution parameters from the sieve analysis (Fig. 13 b), Simulation (sieve analysis)).
It is clearly visible that, the model prediction is in very good agreement with the measured concentration signal (Fig. 13 b), even though the temperature profile (Fig. 13 a) is rather complex. Furthermore, almost the same simulation output is obtained when the estimated parameters for growth and dissolution of the sieve analysis are applied. Small deviations occur only shortly after seeding (t = 0…0.5 h) where the actual growth of the initial crystals is faster than the predicted one. This can be due to attached dust that is growing as well.
Also the simulation of the solid phase evolution (Fig. 13 d) agrees well with the measurements of the online microscopy (Fig. 13 c). The predicted final size of the seed fraction (560 µm applying the kinetics resulting from the online microscopy investigations; 570 µm utilizing the quantified kinetics from the sieve analysis) only deviates by about 20-30 µm from the observations (590 µm).
Nevertheless, nucleated particles are far more pronounced in the simulation results. Either, a higher nucleation rate is predicted or the newly born crystals did not exhibit the same growth rate as the seed crystals during the experiment, an observation which was made during the experiments KAL_1-KAL_{11} as well.

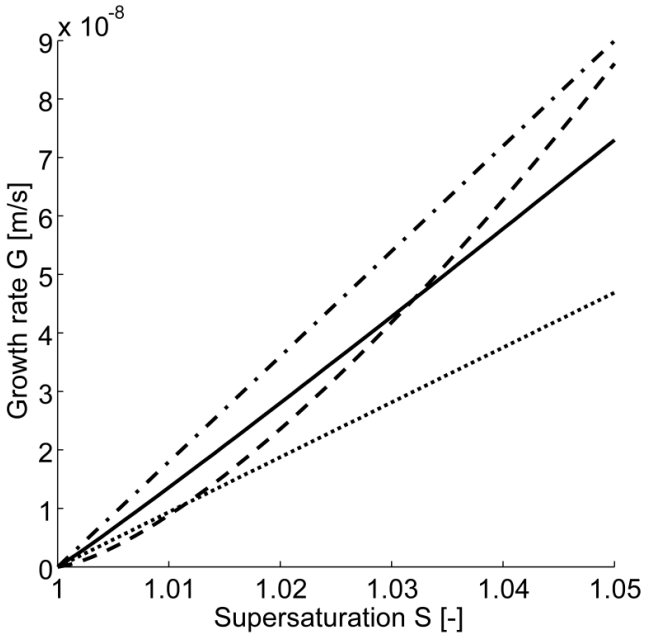

Fig. 14: Comparison of growth kinetics of potassium alum from own measurements with references at T = 302.6 K.
Solid line - growth rate quantified with online microscopy applying eq. 4 and parameters of table 4; *dashed line* - growth rate quantified with sieve analysis applying eq. 4 and parameters of table 4; *dashed-dotted line* - growth rate according to [10] applying a linear approach (eq. 4 with p_2 = 0 & p_3 = 1); *dotted line* - growth rate according to [11] applying a linear approach (eq. 4 with p_2 = 0 & p_3 = 1).

The quantified growth kinetics are in good agreement with data from different references [10, 11] for a temperature of 29.5°C as shown in figure 14. Nevertheless, various studies exist, which quantified completely different growth rates (for a comprehensive summary see e.g. [12]). Thus, it should be stressed again, that numerous parameters influence the quantification of kinetics like e.g. the method itself, the experimental set-up, present impurities and available measurement techniques.

5.4. Model validation for Potassium dihydrogen phosphate

Potassium dihydrogen phosphate (KDP) was chosen as model substance since the shape of the crystals depends significantly on the applied process conditions. If only one crystal dimension (e.g. crystal length or width) is followed during the experimental investigations, a simulation utilizing subsequently estimated parameters, describes just this dimension. Consequently, an error will occur if another dimension is predominant for certain crystallization conditions. Thus, the impact of a changing morphology on the precision of the quantified kinetic rates utilizing the short-cut-method can be investigated. The experimental analysis and the parameter estimation for KDP were carried out in the same way as for KAL.
The images recorded during the validation experiment for KDP (KDP_{Valid}) show that the crystal shape changes remarkably (Fig. 15 a). Nevertheless, the predicted concentration profile (Fig. 15, b) agrees well with the experimental values.

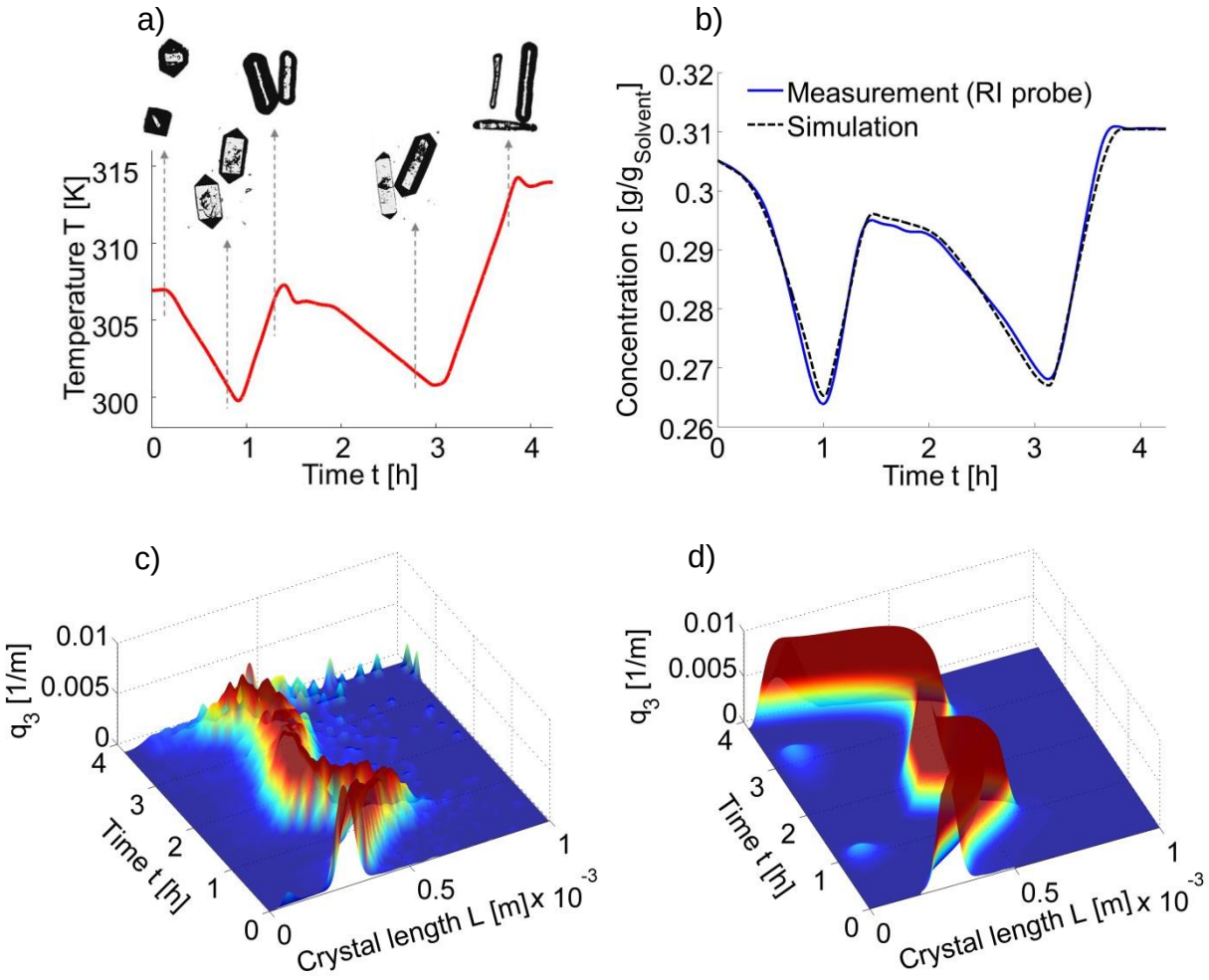

Fig. 15: Measured quantities of the validation experiment KDP_{Valid} in comparison to the model equipped with the estimated parameters from table 5; a) Temperature and observed crystal shapes; b) Measured and simulated concentration profile; c) Observed CSD (online microscopy); d) Predicted solid phase evolution applying the kinetic rates from the online microscopy.

This model prediction was carried out applying a power law combined with an Arrhenius approach for growth (eq. 4), a solid content dependent secondary nucleation sub-model (eq. 5) and a linear temperature independent approach for dissolution (eq. 4). The kinetic parameters obtained during the previous analysis of the experiments (KDP_1 - KDP_4) are given in table 5.

Even though the concentration can be well predicted, deviations in the solid phase evolution between experiment and simulations occur since the volumetric shape factor, k_V, is constant in the calculations. The chosen k_V of 0.75, which is an average of all observed single crystals during experiments KDP_1-KDP_4, best describes crystals with prismatic shapes (Fig. 15 a), t = 0.8 h) but not the bi-pyramidal (Fig. 15 a), t = 0.1 h) or needle like shapes (Fig. 15 a), t = 3.8 h). Thus, the deviations of the seed fraction mean length between simulation and experiment increases from 5 µm (experiment: 530 µm, simulation: 535 µm) after the first crystallization cycle (compare Fig. 15 c) & d) at t = 1 h) to 90 µm (experiment: 440 µm, simulation: 530 µm) after the second cycle (compare

Fig. 15 c) & d) at t = 3 h). These results could be improved by describing the volume shape factor as a function of supersaturation and temperature as well. Nevertheless, this is beyond the scope of this publication and the overall trend of the experiment can be predicted with good agreement applying the determined kinetics.

Table 5: Kinetic parameters estimated using the power-law sub-model (eq. 4) for growth and dissolution and the parameters for the solid content dependent nucleation sub-model (eq. 5) for potassium dihydrogen phosphate applying the CSD results from the online microscopy.

Sampling method	**Exp. (Table 3)**	**Kinetic**	$\mathbf{p_1}$ [m/s; 1/s]	$\mathbf{p_2}$ [kJ/mol; -]	$\mathbf{p_3}$ [-]
Online microscopy	KDP_1-KDP_4	**Growth G**	5.1×10^{6}	70×10^{3}	1.26
		Nucleation B_0	5.2×10^{-2}	5.8	1
		Dissolution D	7.0×10^{-6}	0	1

A comparison with literature data (Fig. 16) yields again a good agreement in particular with references [6, 13] but only a fair agreement with recent studies carried out in the Max-Planck-Institute Magdeburg [5]. Again, a single concrete reason for the deviations cannot be specified, similar to the results of potash alum.

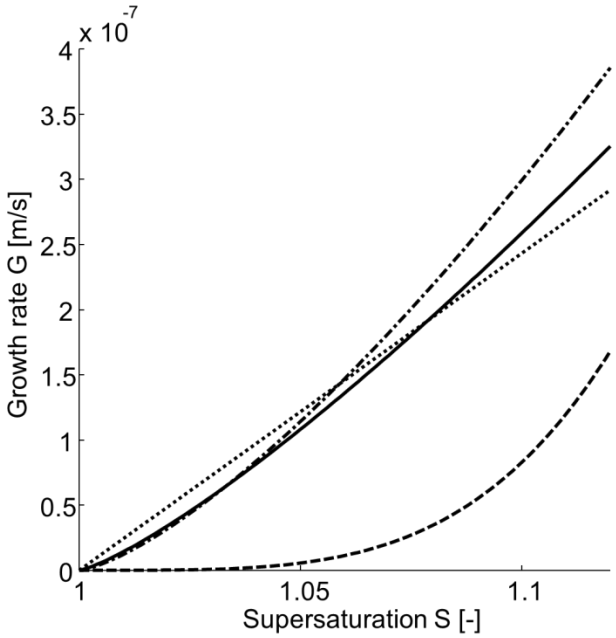

Fig. 16: Comparison of growth kinetics of KDP from own measurements with growth rates of the {100}-faces of different references at T = 303.15 K.
Solid line - growth rate quantified with online microscopy applying eq. 4 and parameters of table 5; *dashed line* - growth rate according to [5] applying a temperature independent power-law (eq. 4 with $p_2 = 0$ & $p_3 = 1$); *dotted line* - growth rate according to [6] applying a temperature dependent linear equation (eq. 4 with $p_3 = 1$); *dashed-dotted line* - growth rate according to [13] applying a temperature independent power-law (eq. 4 with $p_2 = 0$ & $p_3 = 1$).

5.5. Application: quantification of kinetics for ortho aminbenzoic acid

In contrary to the well soluble and well growing substances KDP and KAL, the ortho aminobenzoic acid is a more realistic case. The solubility in water is limited to 1% for the investigated temperature range. Furthermore, part of the crystal phase tends to float on the liquid surface during crystallization/ dissolution experiments due to the low solid density. Additionally, a lot of air bubbles were mixed into the suspension due to these floating crystals. Present crystals exhibited a strong agglomeration tendency regardless whether the process was seeded or not. Also some insoluble impurities were present in the raw material that led, together with the other facts mentioned, to a rather strong scattering of the CSD data acquired with the online microscope.

The liquid phase composition was not measured continuously in this case since the substance seems to decompose in solution over time with a noticeable change of the liquid color from yellow to brown. Thus, the concentration was determined by sampling and offline analysis applying HPLC as described in section 3.2.

Nevertheless, the same data analysis procedure as described above for KAL was applied to experiments $oABA_1$- $oABA_5$. The estimated parameters of the applied temperature independent power-laws are listed in table 6.

Table 6: Kinetic parameters estimated for the power-law sub-model (eq. 4) for ortho aminobenzoic acid applying the CSD results from the online microscopy.

Sampling method	Exp. (Table 3)	Kinetic	p_1 [m/s; 1/s]	p_2 [kJ/mol; -]	p_3 [-]
Online microscopy	$oABA_1$-$oABA_5$	**Growth G**	3.37×10^{-7}	0	1
		Nucleation B_0	1.39×10^{5}	0	2.62
		Dissolution D	5.63×10^{-7}	0	1

It should be noted that in the case of oABA also crystallizations from clear solutions were performed (Table 3) and exploited during parameter estimation since secondary nucleation could not be observed sufficiently. Therefore, also the validation experiment was carried out unseeded to evaluate the so quantified nucleation kinetics. The experimental results from this run are depicted in figure 17. Furthermore, the solid phase was confirmed to be the stable polymorph [14] as expected.

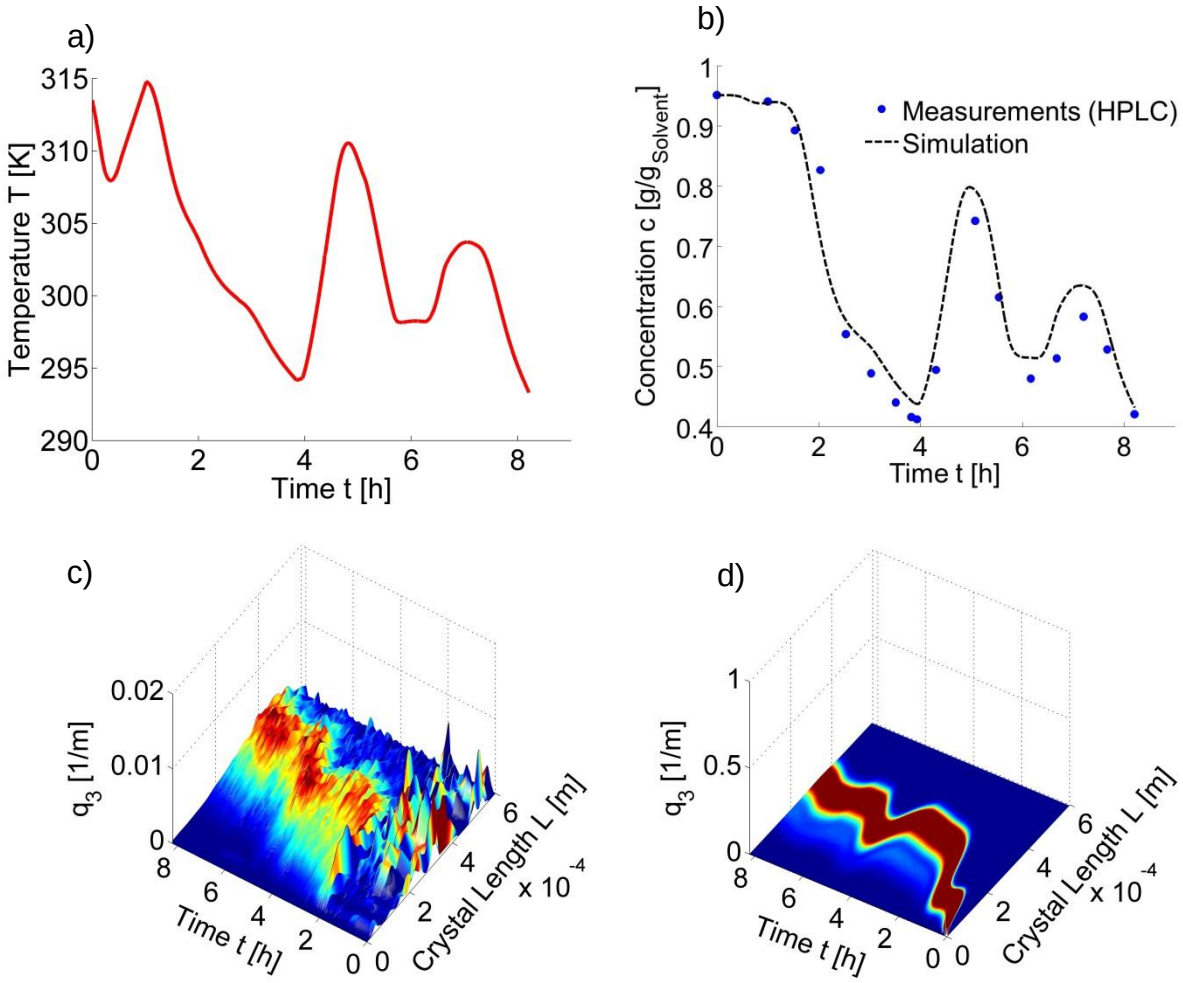

Fig. 17: Measured quantities of the validation experiment $oABA_{Valid}$ in comparison to the model equipped with the estimated parameters from table 6; a) Temperature; b) Measured and simulated concentration profile; c) Observed CSD (online microscopy); d) Predicted solid phase evolution applying the kinetic rates from the online microscopy.

It can be stated, that the model prediction for the concentration agrees with the experimental observations (Fig. 17 b) even for this challenging case. Nevertheless, the deviations are higher than for the other two substances as expected. Especially the predicted dissolution is slightly faster in comparison to the experimental results.
Due to the mentioned measurement noise of the CSD data seen in figure 17 c), it was not possible to observe the initial primary nucleation event and subsequent growth of the early crystals.
The solid phase evolution is first observable after 2 h. After this period the trend of the experiment agrees with the model prediction (Fig. 17 d). Nevertheless, the measured mean product size is 420 µm (t = 8 h) and deviates by about 70 µm from the simulation (mean size 350 µm). Even though, the precision of the predictions is much lower than for the other substances, the quantified rates would be sufficient for a first process design.

5.6. Summary and comparison of the kinetic parameters

The application of the short-cut-method for the quantification of kinetic rates, required in 1-dimensional population balance models, was demonstrated for three different substance systems. The experimental procedure, data analysis and the estimation routine was discussed in detail.

Even though, the short-cut-method is not intended to reveal mechanistic details, accompanying to the summary some remarks regarding the estimated kinetic parameters are given in the following.

It was demonstrated, that crystallization kinetics can be determined with great accuracy for substances like potassium alum with four simple seeded batch experiments. Nevertheless, it was observed that the quantified growth rates of the seed crystals are not necessarily valid for particles that nucleate during the process. Additionally it could be shown, that growth and dissolution kinetics can be quantified utilizing simple sieve analysis with a sufficient degree of accuracy compared to the more sophisticated method employing an online microscope.

Low activation energies were found for nucleation and growth kinetics of potash alum. Thus, a temperature dependency of the corresponding rates can be neglected for the investigated temperature range. The nucleation exponent is close to unity for this substance, which is reasonable if secondary nucleation is dominant. Nevertheless, a secondary nucleation sub-model, which was applied for potassium dihydrogen phosphate (KDP), did not improve the agreement between the simulations and the observed quantities.

For substances, which exhibit drastic morphological shape changes during the process, deviations between model predictions and experimental measurements occur as expected. This was demonstrated for KDP when assuming a constant volume shape factor. It is possible to determine the growth rates of all occurring crystal faces to overcome this problem [5]. However, currently this procedure cannot be applied for more complicated crystal shapes. Thus, a first approach would be to correlate at least the volumetric shape factor with the process conditions.

The activation energy of the growth kinetics of KDP indicates an integration limited mechanism. However, a justified interpretation is difficult due to the correlation of the fitted parameters of equation 4. The secondary nucleation approach (eq. 5) described the particle number evolution best for this substance. Here, the large exponent accounts for a strong solid content-dependency.

The estimated growth exponents are in a range between one and two for all investigated substance systems, which is in agreement with the literature [2] for the chosen growth approach (eq. 4).

The short-cut-method was subsequently also applied to the complicated case of ortho amino benzoic acid, which led to the highest deviations between simulation and experimental observations. The properties of the crystal phase of this substance complicate a precise CSD determination. Furthermore, an inline concentration measurement was not possible in this case. Thus, errors, which are made during the offline analysis of the solution, will influence the precision of the estimates as well. Nevertheless, it could be shown that the concentration during the process can be predicted with acceptable accuracy and that at least the trend of the solid phase evolution can be described even for an unseeded experiment.

The kinetics of oABA were described sufficiently with temperature-independent approaches. Even though, unseeded experiments were utilized for the parameter estimation of the nucleation approach, a rather small exponent was found. Hence, there is evidence that eventually primary and secondary nucleation were observed together.
A physical interpretation of all pre-exponential factors (p_1 in eq. 4) will not be given since they contain several dependencies, which cannot be distinguished from each other.

6. Conclusions

The design of crystallization processes can significantly benefit from the knowledge of growth, dissolution and nucleation kinetics. In this contribution a short-cut-method, investigated theoretically in [4] was validated experimentally. It was shown to be able to quickly and reliably quantify kinetics that can be used for process design. It can be applied if appropriate techniques for concentration, temperature and crystal size distribution measurement are available for the substance system of interest.
Additionally, the growing or dissolving seed fraction and the number of crystals have to be determined accurately. Both can be obscured by other crystallization mechanisms, like agglomeration and breakage.
Hence, the applied measurement techniques and the experimental conditions have to be chosen according to the physical and chemical properties of the substance system in the liquid and solid state as well as with respect to the crystal shape.
The kinetics of the three substance systems can be well predicted and batch-crystallizations with complex temperature profiles can be described as shown by the validation experiments. Thus, the estimated parameters and identified sub-models can be applied for optimization of the process conditions or improving the crystallizer and process design based on PBE models.

Acknowledgements
The experimental work of Nicole Hoyer and Ulrike Grobleben is gratefully acknowledged by the authors.

Andreas Seidel-Morgenstern gratefully acknowledges the support of this research work by the German Research Foundation (DFG) under the grant SE 586/ 20-2 embedded in the Priority Programme SPP 1679.

Symbols & abbreviation

B_0	[1/s]	Nucleation rate
c	[-]	Concentration (mass loading, $g_{Solute}/g_{Solvent}$)
D	[m/s]	Dissolution rate
f	[#/m]	Number density distribution/ function
G	[m/s]	Growth rate
K	[m/s; 1/s]	Kinetic G, B0 or D in (eq. 4)
k_V	[-]	Volume shape factor
L	[m]	Property coordinate corr. to the minimal ferret diameter
$\bar{L}$	[m]	Mean length
M	[kg/m^3]	Solid content
$\tilde{M}$	[g/ mol]	Molar mass
m	[kg]	Mass
N	[#]	Number of crystals
Pr	[%]	Purity
p	[-]	Parameters for the solubility correlation and kinetic laws
$q_{(0, 1, 2, 3)}$	[1/ m]	Relative size distribution with respect to the dimension 0 (amount), 1 (length), 2 (surface), 3 (volume or mass)
ρ	[kg/m^3]	Density
S	[-]	Relative Supersaturation
T	[K]	Temperature
t	[h]	Time
θ	[°C]	Temperature in degree Celsius
V	[m^3]	Volume

Sub- & Superscripts

End/ Final	Final
Est	Estimated
Exp	Experiment
H_20	Water
Liquid	Liquid phase
Min	Minimal
Reactor	Reactor
Sample	Sample
Sat	Saturation
Seeds	Seed
Sim	Simulated
Solid	Solid phase
Solute	Solute
Solvent	Solvent
0	Initial value
*	Saturation

References

[1] Garside, J.; Mersmann. A.; Nývlt, J.; *Measurement of Crystal Growth Rates*, European Federation of Chemical Engineering, Working Party on Crystallization, Germany, 1990, Vol. 1.

[2] Mullin, J. W., *Crystallization*, Butterworth-Heinemann, Boston, 1997, Vol. 3.

[3] Nývlt, J., Söhnel, O., Matuchová, M., Boul, M., *The Kinetics of Industrial Crystallization*, Elsevier Science Publishers, Amsterdam, 1985.

[4] Temmel, E.; Eisenschmidt, H.; Lorenz, H.; Sundmacher, K.; Seidel-Morgenstern, A. *A short-cut-method for the quantification of crystallization kinetics - Part1: Method development* - submitted to *Cryst. Growth Des.*.

[5] Borchert, C.; Temmel, E.; Eisenschmidt, H.; Lorenz, H.; Seidel-Morgenstern, A.; Sundmacher, K. *Cryst. Growth Des.*, 2014, 14, 952-971.

[6] Eisenschmidt, H.; Voigt, A.; Sundmacher, K. *Cryst. Growth Des.*, 2015, 15, 219-227.

[7] Borchert, C.; Sundmacher, K. *Chem. Eng. Technol.*, 2011, 34, 545-556.

[8] Binev, D.; *Continuous fluidized bed crystallization*, Dissertation, Otto von Guericke University, Magdeburg, 2015.

[9] Gahn, C.; *Die Festigkeit von Kristallen und ihr Einfluß auf die Kinetik in Suspensionskristallisatoren*, Dissertation, Herbert Utz Verlag, Munich, 1997.

[10] Girolami, M. W.; Rousseau, R. W. *J. Cryst. Growth*, 1985, 71, 220-224.

[11] Mullin, J. W.; Garside, J. *Trans. Inst. Chem. Engrs*., 1967, 45, T291.

[12] Mohan, R.; Myeson, A. S. *Chem. Eng. Sci.*, 2002, 57, 4277-4285.

[13] Gunawan, R.; Ma, D. L.; Fujiwara, M.; Braatz, R. D. *Int. J. Mod. Phys. B*, 2002, 16, 367-374.

[14] Jiang, S.; Jansen, P. J.; ter Horst, J. H. *Cryst. Growth Des.*, 2010, 10, 2541-2547.

Appendix

Potash alum ($KAl(SO_4)_2 \cdot 12H_2O$, KAL) was purchased from Applichem with a purity of >99.5%. It crystallizes from water at ambient conditions as a dodecahydrate in a cubic lattice with the space group Pa3. The crystal shape is dominated by the slow growing {111} faces but sometimes also the {100} and {110} faces were observed (Fig. 5). A correlation between the occurrences of the faces with the process conditions was not found.
The shape was assumed to be a perfect octahedron even though {100} and {110} faces were frequently observed. The characteristic length, L, was chosen to be the edge length of the base of the octahedron (second largest elongation) since this would be the measured mesh size of a sieve analysis (Fig. A.1). Therefore, the volumetric shape factor, k_V, can be calculated with simple geometrical equations to $\sqrt{2}/3$ (Table 1).

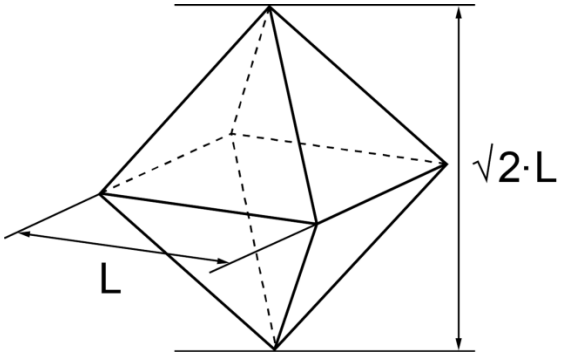

Fig. A.1: Assumed shape of KAL for the calculation of the shape factor k_V.

Potassium dihydrogen phosphate (KH_2PO_4, KDP) was purchased from Carl Roth with a purity of >98%. The substance crystallizes as an anhydrate with a tetragonal lattice at room temperature and belongs to the space group I-42d. The substance crystallized from water forms prisms ({100} faces) with pyramidal ends ({101} faces). The corresponding volume shape factor is consequently dependent on the process conditions as well. Hence, this substance serves for the proposed short-cut-method to investigate the accuracy of the estimated kinetics with respect to shape changes of the substance of interest since the task is to parameterize simple 1-dimensional PBE models. Similar to KAL the distributor and the corresponding batch of the bought KDP had to be one and the same to ensure a constant impurity matrix of the initial material.

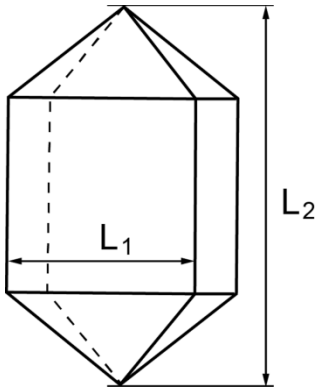

Fig. A.2: Assumed shape of KDP for the calculation of the shape factor k_V.

The volume of a KDP crystal consists of the volume of two pyramids and one cuboid (Fig. A.2). The heights of the pyramidal ends are related to the edge length of the cross section of the cuboid via equation A.1.

$$h_{pyr} = \frac{c}{2a} L_1 \qquad \text{(eq. A.1)}$$

Where *c* and *a* are the tetragonal lattice parameters of KDP (I-42d). Thus, the volume of a KDP crystal can be calculated via:

$$V_{KDP} = V_{cub} + 2V_{pyr} = L_1^2 L_2 - \frac{2}{3}\frac{c}{a} L_1^3 \qquad \text{(eq. A.2)}$$

Therefore, the shape factor depends on two dimensions and cannot be calculated based on the second biggest dimension alone. Hence, online microscopy was applied to evaluate a high amount of particles with respect to L_1 and L_2 (eq. A.2).

Ortho aminobenzoic acid ($C_7H_7NO_2$, oABA) was bought from VWR with a purity of >99%. A perfect rhombic plate with height *L* (Fig. A.3) was assumed for the calculations of the shape factor.

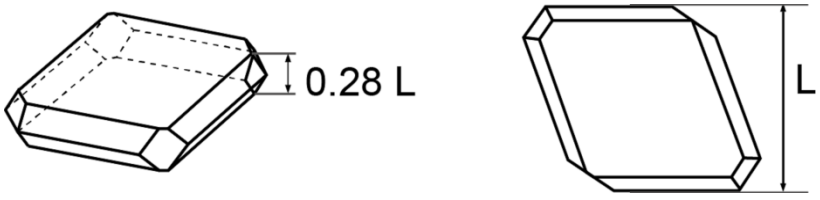

Fig. A.3: Assumed shape of oABA for the calculation of the shape factor k_V.

Several crystals were investigated with an offline microscope to determine the ratio of both dimensions as well as the angles of the rhomboid. The large angle was found to be 110° (±1.13) and the ratio between the characteristic length *L* and the crystal thickness

determined to be 0.28 even though the standard deviation is relatively large (±0.05). Hence, the volume of the oABA crystals can be calculated via:

$$V_{oABA} = 0.28\frac{L^3}{\sin(110°)} \qquad \text{(eq. A.3)}$$

For Table of Contents Use Only

Title:
A short-cut-method for the quantification of crystallization kinetics - Part 2: Experimental application

Authors:
Erik Temmel, Matthias Eicke, Heike Lorenz, Andreas Seidel-Morgenstern

Synopsis:
The short-cut-method for the estimation of crystallization kinetics is evaluated experimentally. Sub-models for nucleation, growth and dissolution are parameterized for three different substances dissolved in water: Potassium aluminum sulfate, potassium dihydrogenphosphate and ortho aminobenzoic acid. The quantified kinetics are subsequently validated by batch-experiments with complex temperature profiles.

TOC graphic